Zeolites

DOI: 10.1002/anie.201105678

Highly Stable and Reusable Multimodal Zeolite TS-1 Based Catalysts with Hierarchically Interconnected Three-Level Micro–Meso–Macroporous Structure**

Li-Hua Chen , Xiao-Yun Li, Ge Tian, Yu Li, Joanna Claire Rooke, Guang-Shan Zhu, Shi-Lun Qiu, Xiao-Yu Yang, and Bao-Lian Su**

Microporous titanosilicates, such as TS-1, are a class of important catalysts with high activities and selectivities coupled with environmentally benign catalytic performance, and play a vital role in a series of catalytic oxidation reactions with H_2O_2.[1] However, an important drawback of these titanosilicate catalysts is that their pores are too small to be accessed by bulky reactants, and this hinders their use in the fine-chemical and pharmaceutical industries.[2] Nanosized TS-1 materials were initially considered as a potential approach to improving the accessibility of such catalysts because, owing to their larger external surface areas, they have more active sites than conventional zeolites. However, complex processes for their separation from reaction products and the ease of aggregation of the nanosized zeolites during synthesis and catalytic reactions limit seriously their development.[3] Recent progress in the field has seen the incorporation of titanium ions into the framework of mesoporous materials[4,5] and grafting of a titanocene complex onto mesoporous silica.[6] These ordered mesoporous titanosilicates have pore diameters of 2–8 nm and exhibit catalytic properties for the oxidation of bulky reactants under mild conditions. Unfortunately, when compared with TS-1, their catalytic activity, for example, that of Ti-MCM-41, is relatively low. This is attributed to the difference in the titanium coordination environment (amorphous nature of the mesoporous wall).[7] A series of ordered mesoporous titanosilicates have been synthesized by assembly of preformed titanosilicate zeolite precursors with triblock copolymers, and showed good activity in the oxidation of small molecules such as phenol and styrene as well as bulkier molecules like trimethylphenol.[8] However, calcination leads to a significant reduction in catalytic activity towards both small and bulky molecules, due to the relatively low stability of catalytically active four-coordinate titanium sites in these materials[7] compared to those in TS-1. The relatively low stabilities of both the titanium species and the structure in catalytic processes may be related to imperfectly condensed mesoporous walls. Possibly, the degree of crystallization of the mesoporous walls should be enhanced. Therefore, mesoporous titanosilicates with an fully crystalline structure are highly desirable.

Novel 3D crystalline metallosilicates with expanded pores were recently synthesized from 2D Ti-MWW (MWW-type titanosilicate) precursors,[9] according to a strategy of inserting a monomeric Si source into the interlayer spaces. The resultant materials showed expanded pore apertures, high crystallinity, and outstanding redox catalytic properties towards bulky molecules. Consequently, increasing the pore size has been one of the goals of structural control, to permit the penetration of large molecules into the host porous structure. Macroporous titanosilicates with crystalline structure are particularly interesting, due to their improved transport properties.[10] Well-defined macroporous arrays should show optimal fluxes, whereby diffusion is not a limiting issue. Therefore more efficient catalysts could be targeted through the controlled design of hierarchically meso–macroporous titanosilicates with crystalline structure, principally by introducing the multipore system evenly throughout the framework. The ideal hierarchically porous structure in efficient titanosilicate catalysts should contain a macropore system to enhance mass transport, mesopores for precise selectivity, and microporous zeolitic structure to provide the catalytically active sites. More attractive applications could be developed if new titanosilicate catalysts could be constructed with hierarchical micro–meso–macropore systems yet still be composed of the same highly active

[*] Dr. L.-H. Chen , Dr. Y. Li, Dr. X.-Y. Yang, Prof. B.-L. Su
State Key Laboratory of Advanced Technology for Material Synthesis and Processing, Wuhan University of Technology
Luoshi Road 122, Wuhan 430070 (China)
E-mail: xyyang@whut.edu.cn
baoliansu@whut.edu.cn

Dr. L.-H. Chen , X.-Y. Li, Dr. G. Tian, Dr. J. C. Rooke, Dr. X.-Y. Yang, Prof. B.-L. Su
Laboratory of Inorganic Materials Chemistry (CMI)
University of Namur (FUNDP)
61, rue de Bruxelles, 5000 Namur (Belgium)
E-mail: xyyang@fundp.ac.be
bao-lian.su@fundp.ac.be

Dr. L.-H. Chen , Prof. G.-S. Zhu, Prof. S.-L. Qiu
State Key Laboratory of Inorganic Synthesis & Preparative Chemistry, Jilin University
2699 Qianjin Street, Changchun 130012 (P. R. China)

[**] This work was supported by the frame of a Belgian Federal Government (Belspo PAI-IAP) project (INANOMAT, P6/17), the Belgium-Viet Nam bilateral cooperation project (BL/13V11), CSC (China Scholarship Council) for the State Scholarship Fund, FNRS (Fonds National de la Recherche Scientifique in Belgium) for a "Chargé de recherche" position, the Chinese Hubei government for a "Chutian chair scholar" honor, the Chinese Central Government for an "Expert of the state" position in the frame of "Thousand talents program", the Chinese Ministry of Education for a "Chang jiang chair visiting scholar" position at Wuhan University of Technology.

Supporting information for this article is available on the WWW under http://dx.doi.org/10.1002/anie.201105678.

framework units found in current materials such as MFI structures.

Herein we describe the synthesis of a new type of hierarchical micro–meso–macroporous zeolitic TS-1 architectures by a crystallization process in a quasi-solid-state system. All pores, over three length scales, were incorporated throughout the final solid body to give a highly interconnected network of well-defined macrochannels with uniform mesoporosity and zeolitic microchannels. The titanosilicate catalysts not only contain thermally stable TS-1 nanocrystals with meso–macroporous structure, but they also show high thermal stability themselves. The recyclability of the catalysts was demonstrated by regeneration of catalytically active four-coordinate titanium sites in the TS-1 nanocrystals. The synthesis of hierarchical micro–meso–macroporous catalysts constructed from uniform TS-1 zeolite nanoparticles is illustrated in Figure 1. First, hierarchically meso–macroporous titanosilicates with amorphous architecture (Figure 1a) were synthesized by a spontaneous procedure without any external templates[11] and subsequently used as the precursors for the next step. These precursors were then impregnated in a suspension containing the zeolite MFI structure-directing agent tetrapropylammonium ion (TPA^+) and an additional silica source tetraethyl orthosilicate (TEOS), which facilitated transformation of the amorphous phase of the meso–macroporous precursors into crystalline micro-meso–macroporous catalysts with zeolitic architecture. A gel was obtained after removing the water from the suspension under vacuum. The structure-directing agent TPA^+ and the TEOS molecules were dispersed into the mesopores of the precursors by a rotary evaporation process (Figure 1b). Subsequently, a quasi-solid-state system was formed by mixing the gel with a glycerol medium. The crystallization process was then initiated owing to the influence of TPA^+ under the quasi-solid-state conditions as it aged at 130 °C. The amorphous hierarchical titanosilicate precursor was gradually transformed into a crystalline material with zeolite TS-1 architecture by this crystallization process and the meso–macropore structure was preserved owing to this quasi-solid-state system, as illustrated in Figure 1c–e. Aggregates of nanosized zeolite TS-1 crystals were formed under the effect of the structure-directing agent TPA^+ from the amorphous titanosilicate and TEOS (Figure 1d). These zeolite nanoparticles, located in the macropore walls, continued to grow and become more crystalline, resulting in hierarchically micro–meso–macroporous TS-1 (Figure 1e). Samples with different crystallization times are named MMM-TS-1(0) (initial precursor), MMM-TS-1(1) (1 d), MMM-TS-1(2) (2 d), and MMM-TS-1(3) (3 d).

The synthetic process was monitored by SEM (Figure 2) and TEM (Figure 3) techniques. Figure 2a and b reveal that the initial precursors had a well-defined macropore structure with a pore size around 1 μm. The macropores were constructed from amorphous nanoparticles, as evidenced by the absence of diffraction peaks in the wide-angle XRD pattern (Figure 4A a), which led to the formation of an interconnected mesoporous system. The products obtained over various crystallization periods retained the well-defined macroporous structures with interconnected mesopores (Fig-

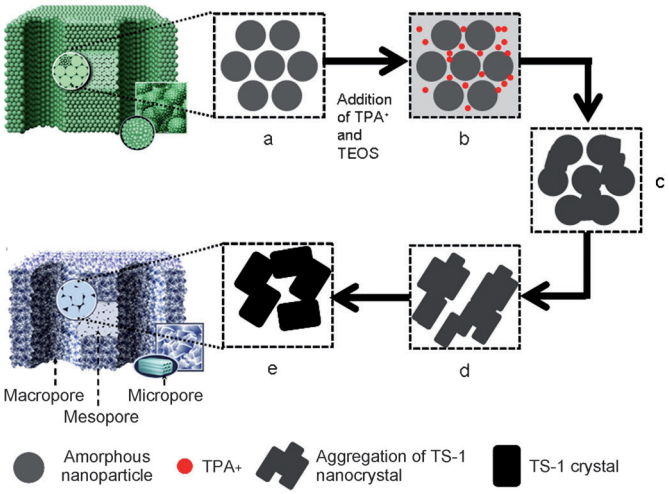

Figure 1. Schematic of the synthetic procedure for hierarchically micro–meso–macroporous catalysts constructed from zeolite TS-1 nanocrystals by a quasi-solid-state crystallization process.

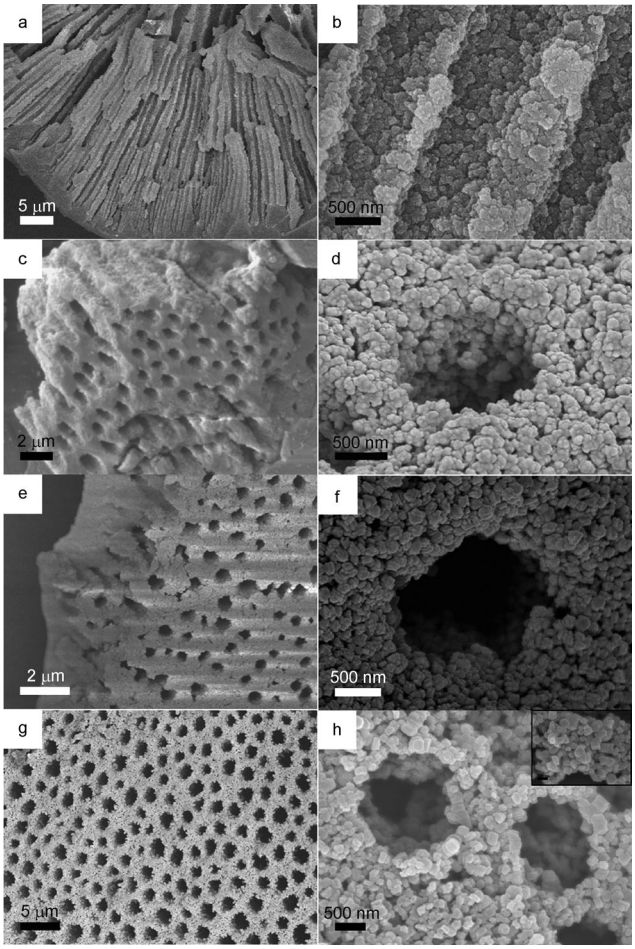

Figure 2. SEM images of products obtained after various crystallization periods. a, b) MMM-TS-1(0); c, d) MMM-TS-1(1); e, f) MMM-TS-1(2); g, h) MMM-TS-1(3).

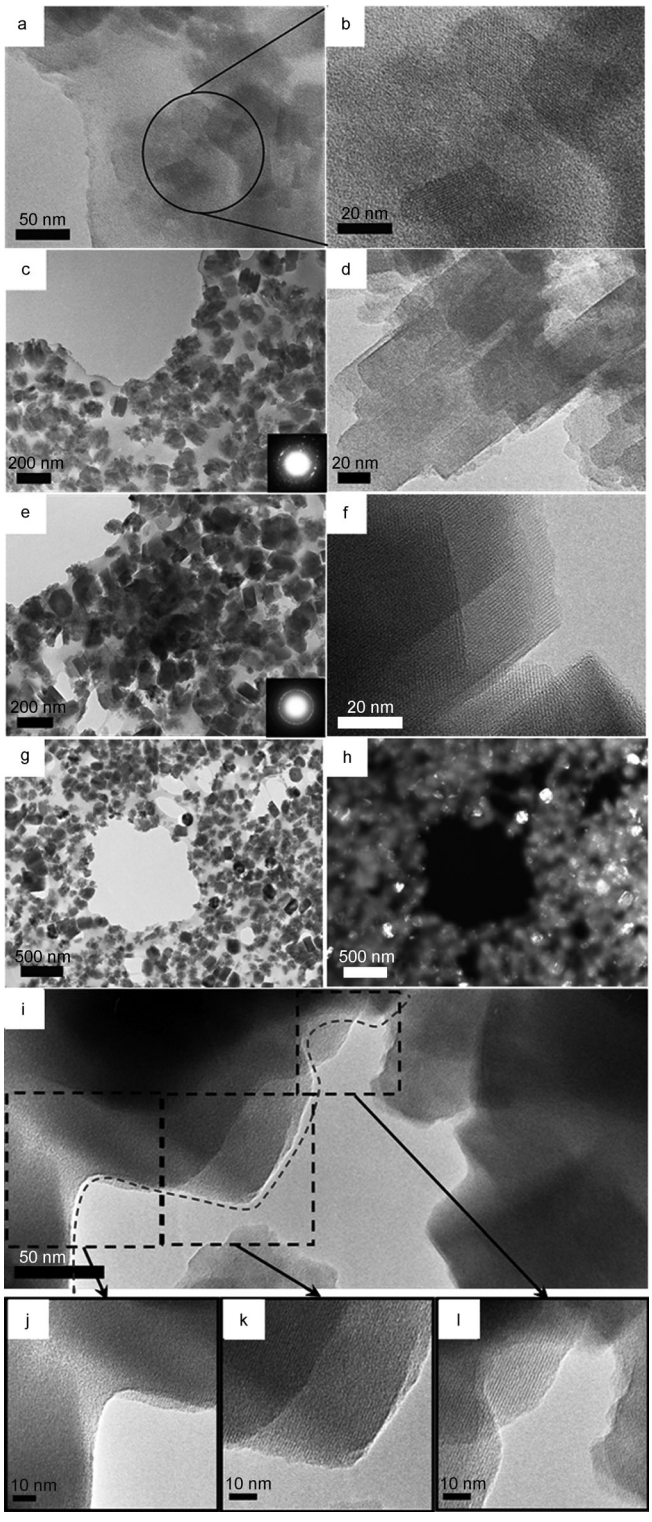

Figure 3. TEM images of products obtained after various crystallization periods. a, b) MMM-TS-1(1); c, d) MMM-TS-1(2); e–l) MMM-TS-1(3).

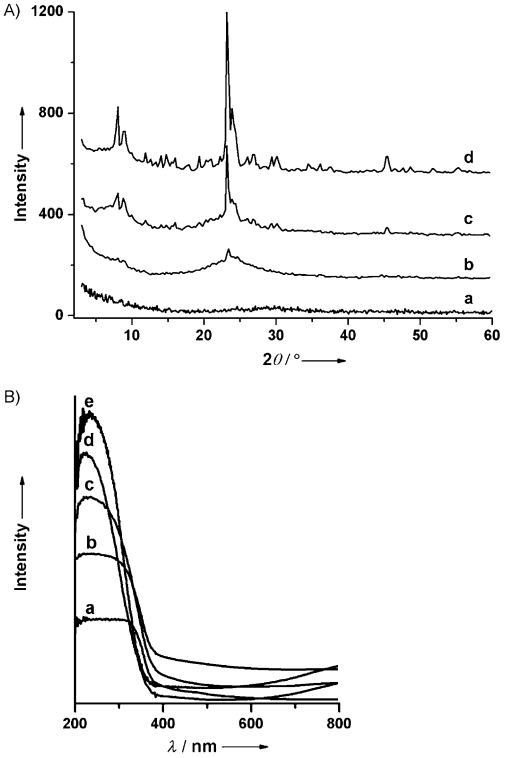

Figure 4. Wide-angle XRD patterns (A) and UV/Vis spectra (B) of the products obtained after various crystallization periods. a) MMM-TS-1(0), b) MMM-TS-1(1), c) MMM-TS-1(2), d) MMM-TS-1(3), and e) recycled MMM-TS-1(3).

ure 2c–f), even after 3 days (Figure 2g). The changes in morphology and crystallinity of the nanoparticles in the walls of the macropores of the products were observed by high-resolution (HR) SEM and TEM. The HRTEM image (Figure 3a and b) clearly showed that some small nanoparticles with zeolite MFI structure had formed and were embedded within the framework of the MMM-TS-1(1) product, which still had a mainly amorphous architecture. As the process proceeded, larger nanoparticles, consisting of several fused nanocrystals, formed in the macropore walls of product MMM-TS-1(2) (Figure 2f). High-resolution TEM images confirmed that these larger particles were aggregates of TS-1 nanocrystals which replaced the initial spherical nanoparticles (Figure 3c and d). These zeolite nanoparticles, located in the macropore walls, continued to grow and become more crystalline. The macropore walls of the MMM-TS-1(3) product were completely constructed from highly crystalline zeolite nanocrystals of uniform size (Figure 2h and 3f). It is noteworthy that the zeolite TS-1 architecture in the final products exhibited a uniform particle size of around 200 nm (Figure 2h, Figure 3e, and Figure 3g), resulting in relatively uniform mesovoids (4.8 nm), as evidenced by the mesopore size distribution obtained through N_2 adsorption/desorption measurements (Figure S3, Supporting Information). The formation of zeolite TS-1 nanocrystals with uniform size could be attributable not only to the competitive growth of each crystal, but also to the interaction between zeolite nanocrystals, which led to a confined-space effect. In addition, the relatively mild glycerol system employed in the chemical crystallization process was also a potential reason why uniform particles were more likely to form due to the possibility of slowing down the growth rate under these conditions. The circular streaking in the electron diffraction

pattern (inset of Figure 3e) also indicated that the MMM titanosilicates were constructed from randomly orientated, highly crystalline zeolite TS-1 nanocrystals. The Si/Ti ratio in the MMM-TS-1(3) final product was 104, as characterized by energy-dispersive X-ray analysis (EDS) and inductively coupled plasma (ICP) analysis. The dark-field image (Figure 3h), acquired on the same region as the bright-field TEM image (Figure 3g), further indicated that the meso–macroporous framework of the final product was mainly crystalline, owing to the presence of bright spots corresponding to TS-1 nanocrystals which fully occupied the matrix. The well-defined macropore structure and interconnected mesoporous systems were successfully retained in this quasi-solid-state system (see Figure 2g and h). This may be attributable to the presence of glycerol, a clear viscous liquid with low vapor pressure, which may have ensured that the reaction proceeded slowly and thus slowed down the crystallization process. This in turn could avoid the collapse of the hierarchically porous framework, which would ordinarily be damaged in a traditional hydrothermal system with high vapor pressure. Moreover, the glycerol medium became more fluidlike as it was heated and thus acted as a flux improving the interaction between structure-directing agents and growing crystal domains. In this case, the microporous zeolite crystals were able to grow by using the amorphous titanosilicate material and additional TEOS as titanium and silicon sources under the action of the structure-directing agent TPA^+.

Most importantly, even after calcination at 550 °C for 5 h, the nanocrystals in the macroporous walls did not obviously aggregate together. Direct evidence can be observed by HRTEM (Figure 3i). The TEM study of large particle aggregates not only further confirmed that each zeolite nanocrystal had a highly microporous crystalline zeolite MFI structure (see Figure 3k and l for magnified images corresponding to the regions highlighted in Figure 3i), but also showed that the large particle aggregates were constructed from zeolite nanocrystals which were bonded together by the interconnecting amorphous region (Figure 3j). This is a unique structure, which results in greatly improved stability of the hierarchically porous structure and is also a critical factor in avoiding collapse of the macropore walls in the final product. Thus, the amorphous structure in the precursors was gradually transformed into a crystalline zeolitic structure with increasing aging time, as was also confirmed by wide-angle XRD patterns (Figure 4A) and ^{29}Si MAS NMR (Figure S1, Supporting Information) spectroscopic studies. The amorphous phases in the meso–macroporous titanosilicate precursors gradually disappeared, and the crystallinity of the products was enhanced, as evidenced by the development of diffraction peaks corresponding to zeolite MFI structure in the wide-angle XRD pattern, which became more intense as the reaction progressed (Figure 4A). The XRD profile of the MMM-TS-1(3) final product (Figure 4Ad) revealed that a zeolite MFI structure was obtained with a high degree of crystallinity. The ^{29}Si MAS NMR spectrum of the final product showed a highly intense resonance at −112 ppm and a shoulder at −102 ppm, indicating that the framework consisted primarily of cross-linked Q^4 and Q^3 silica units, as deduced from a very high Q^4/Q^3 ratio of 4.8. The N_2 isotherms of the calcined products over various crystallization periods changed from type IV to type I with increasing reaction time (Figure S2, Supporting Information), and this also indicates gradual generation of microporosity in the products. The final material MMM-TS-1(3) exhibited a type I isotherm with hysteresis at the highest P/P_0 ratios (0.95–1.00) which signifies the presence of microporosity and larger interparticle mesoporosity (Figure S2d, Supporting Information).

The titanium species are incorporated into the framework of crystalline zeolite TS-1 in tetrahedral coordination states, which is regarded as the key factor in their catalytic activity.[12,13] The coordination states can be studied by UV/Vis spectroscopy (Figure 4B). The UV/Vis spectrum showed the presence of considerable amounts of anatase and octahedral Ti species in the initial meso–macroporous titanosilicate precursors, as evidenced by a shoulder band around 330 nm (Figure 4Ba). As the process proceeded, the coordination states of Ti species gradually changed from anatase or octahedral to tetrahedral species, which was evidenced by the change in the reflectance bands from 330 and 260 to 220 nm (Figure 4B). Notably, the Ti species in the MMM-TS-1(3) final product (Figure 4Bd) and recycled MMM-TS-1(3) (Figure 4Be) were mainly located in tetrahedral coordination states, as evidenced by the intense band at 220 nm, which suggested that not only had the amorphous Ti species been transformed into a tetrahedral coordination state and incorporated into the final MMM framework, but also that the tetrahedrally coordinated Ti species were stable and reusable during catalytic processes and thermal treatment.

Table 1 presents catalytic activities of MMM-TS-1(3) and nanosized TS-1 in the epoxidation of styrene and 2,4,6-

Table 1: Catalytic activities for the epoxidation of styrene and 2,4,6-trimethylstyrene over normal TS-1 nanocrystals and MMM-TS-1(3) products, and structural parameters obtained through BET for various samples.

Sample[a]	Conv. [%]	S_{BET} [$m^2 g^{-1}$]	Si/Ti ratio	Products [%] P1	P2	P3	P4	P5	P6	P7
S_1[b]	72	260	98	9.5	63.5	4.0	9.5	13.5	–	–
S_2[b]	85	580	104	–	82.4	17.6	–	–	–	–
S_1[c]	5	260	98	100	–	–	–	–	–	–
S_2[c]	45	580	104	50	10.3	6.8	10	5.4	14	3.5
S_2[c, d]	31	580	104	49	9.7	8.3	10.1	6.1	14.4	2.4

[a] All samples were calcined at 550 °C for 5 h. S1: TS-1 nanocrystals. S2: MMM-TS-1(3). [b] Styrene epoxidation: 10% catalyst, styrene:H_2O_2 = 1:2, reaction time = 8 h, products: styrene oxide (P1), benzaldehyde (P2), benzoic acid (P3), 1-phenylethane-1,2-diol (P4), others (P5). [c] : 10% catalyst, 2,4,6-trimethylstyrene:H_2O_2 = 1:2, reaction time = 8 h, products: 2,4,6-trimethylstyrene oxide (P1), 2,4,6-trimethylbenzenecarboxylic acid (P2), 2,4,6-trimethylbenzaldehyde (P3), 2,4,6-trimethylacetophenone (P4), 2,4,6-trimethylphenylacetic acid (P5), 2,4,6-trimethylphenylacetaldehyde (P6), others (P7). [d] Sample was recycled after being calcined at 550 °C for 5 h and reused in 2,4,6-trimethylstyrene epoxidation.

trimethylstyrene. Styrene conversion with MMM-TS-1(3) catalyst can reach 85%, which was higher than that obtained over normal TS-1 nanocrystal catalysts (72%). This is directly attributed to the higher surface area of MMM-TS-1(3) of 580 $m^2 g^{-1}$ compared to TS-1 nanocrystals (260 $m^2 g^{-1}$), and also the well-defined meso–macroporous structure. Furthermore, the selectivity of MMM-TS-1(3) catalysts was far superior to that of TS-1 nanocrystals. Only benzaldehyde and benzoic acid were obtained in the epoxidation of styrene over MMM-TS-1(3) catalysts. One possible reason is that a greater uniformity in the mesopores of MMM-TS-1(3) catalysts may act as the key factor for the selectivity during the catalytic process. Noteworthily, the conversion in the epoxidation of larger molecules (2,4,6-trimethylstyrene) with MMM-TS-1(3) as catalyst reached 45%, as opposed to just 5% for TS-1 nanocrystals, as 2,4,6-trimethylstyrene molecules are too large to enter the micropore channels of the nanocrystals. The MMM-TS-1(3) catalyst has a much larger external surface area due to the presence of mesopores, which means many more active sites exist in this catalyst than in TS-1 nanocrystals. Meanwhile, macropores facilitate penetration of reactants.

Most importantly, the recycled active sites of Ti species in MMM-TS-1(3) still show comparable activities to that of the initial cycle. For example, after recycling by calcination at 550°C for 5 h, the Ti species in MMM-TS-1(3) still exhibit 80% conversion in the epoxidation of styrene, and 31% in the epoxidation of 2,4,6-trimethylstyrene. In contrast, the Ti species in normal TS-1 nanocrystals, often used as reference catalysts[14] for similar reactions, show relatively low activities, due to their ready aggregation.[3,14] The active Ti species in MMM-TS-1(3) are stable, reusable, and active, which can be attributed to its unique and stable hierarchically micro–meso–macroporous structure. The nanosized TS-1 fused together by interconnecting amorphous regions were well dispersed, and the presence of an amorphous phase minimized aggregation of TS-1 nanocrystals, while the meso–macroporous structure favored diffusion of reagents and products.

In summary, we have prepared and characterized a new type of hierarchical micro–meso–macroporous catalysts within zeolite TS-1 architecture by a chemical crystallization process in a quasi-solid-state system. These catalysts show a well-defined macroporous structure and a highly interconnected mesoporous network constructed from zeolite TS-1 nanocrystals with uniform particle size. A hierarchically micro–meso–macroporous structure with improved stability, especially in comparison to TS-1 nanocrystals, was obtained by this chemical crystallization process. The novel hierarchical pore structure and improved stability result in catalysts that exhibit superior catalytic performances compared to normal zeolite TS-1 nanocrystals, especially for the epoxidation of larger molecules. Furthermore, this methodology of crystallization under quasi-solid-state conditions can be developed to synthesize a series of similar hierarchically micro–meso–macroporous catalysts with various types of zeolitic architectures.

Experimental Section

Typical synthetic procedure: First, hierarchical meso–macroporous titanosilicates with amorphous structure were synthesized by dropping a mixture of titanium isopropoxide (10 g, Aldrich, 97% etc.) and tetramethyl orthosilicate (TMOS) (4 g, Aldrich.) into 300 g distilled water, basified to pH 11 with NaOH, at 40°C. The solid products were dried at 60°C and used as precursors for the next step. These precursors (1 g) were impregnated with a homogeneous mixture consisting of 10 g TPA^+OH^- (25%), 10 g TEOS, and 100 g H_2O for 3 h with stirring at room temperature. After heating at 50°C under vacuum to remove the water from the mixture, the gel was mixed with 5 mL of glycerol, transferred to a Teflon-lined autoclave, and aged at 130°C for different time periods (see text for details). After aging, the products were washed with distilled water and dried at 60°C. The final products were obtained after calcining at 550°C for 4 h to remove any organics.

Catalysis studies: The catalytic properties of the final product MMM-TS-1(3) were initially assessed by using the well-known probe reaction of styrene epoxidation. The catalytic activities of all samples were tested for styrene epoxidation with H_2O_2 as an oxidant. Styrene epoxidation was carried out with vigorous stirring in a two-neck Pyrex reactor equipped with a condenser and a thermometer using 1.04 g substrate, 104 mg catalyst, 5 mL acetonitrile as solvent, and 2.2 g of 35% H_2O_2. Substrate:solvent = 1:5, 10 wt% catalyst with respect to substrate, and substrate:H_2O_2 = 1:2. The reaction was conducted at 343 K for 8 h and the product was analyzed by GC-MS. Normal zeolite TS-1 nanocrystals with a molar ratio of Si:Ti ≈ 98 were used as reference in the investigation of the catalytic properties of the MMM-TS-1(X) products. 2,4,6-Trimethylstyrene was used as a test compound to investigate the superior catalytic performance of MMM-TS-1(3) in the epoxidation of larger organic molecules. The reaction conditions were similar to those used in the epoxidation of styrene, but substrate:solvent = 1:10, 10 wt% catalyst with respect to the substrate, and substrate:H_2O_2 = 1:2.

Received: August 10, 2011
Published online: October 5, 2011

Keywords: crystal growth · heterogeneous catalysis · mesoporous materials · microporous materials · zeolites

[1] a) M. Taramaso, G. Perego, B. Notari, US Patent 4410501, **1983**; b) D. R. C. Huybrechts, L. DeBruycker, P. A. Jacobs, *Nature* **1990**, *345*, 240–242; c) T. Tatsumi, M. Nakamura, S. Negishi, H. Tominaga, *Chem. Commun.* **1990**, 476–477; d) B. Notari, *Adv. Catal.* **1996**, 41, 253–334; e) A. Tuel, *Zeolites* **1996**, *16*, 108–117; f) S. Bordiga, A. Damin, F. Bonino, G. Ricchiardi, A. Zecchina, R. Tagliapietra, C. Lamberti, *Phys. Chem. Chem. Phys.* **2003**, *5*, 4390–4393; g) C. Lamberti, S. Bordiga, A. Zecchina, G. Artioli, G. Marra, G. Spano, *J. Am. Chem. Soc.* **2001**, *123*, 2204–2212; h) P. Ratnasamy, D. Srinivas, H. Knözinger, *Adv. Catal.* **2004**, *48*, 1–169.

[2] a) A. Corma, *Chem. Rev.* **1997**, *97*, 2373–2419; b) C. T. Kresge, M. E. Leonowicz, W. J. Roth, J. C. Vartuli, J. S. Beck, *Nature* **1992**, *359*, 710–712; c) J. X. Jiang, J. H. Yu, A. Corma, *Angew. Chem.* **2010**, *122*, 3186–3212; *Angew. Chem. Int. Ed.* **2010**, *49*, 3120–3145.

[3] a) Y. S. Tao, H. Kanoh, L. Abrams, K. Kaneko, *Chem. Rev.* **2006**, *106*, 896–910; b) P. R. Javier, H. C. Claus, E. Kresten, H. C. Christina, C. G. Johan, *Chem. Soc. Rev.* **2008**, *37*, 2530–2542.

[4] a) A. Corma, M. A. Camblor, P. Esteve, A. Martinez, J. Perez-Pariente, *J. Catal.* **1994**, *145*, 151–158; b) P. T. Tanev, M. Chibwe, T. J. Pinnavaia, *Nature* **1994**, *368*, 321–323; c) S. A. Bagshaw, E. Prouzet, T. J. Pinnavaia, *Science* **1995**, *269*, 1242–1244; d) W. Zhang, M. Fröba, J. Wang, P. T. Tanev, J. Wong, T. J. Pinnavaia, *J.*

Am. Chem. Soc. **1996**, *118*, 9164 – 9171; e) K. A. Koyano, T. Tatsumi, *Chem. Commun.* **1996**, 145 – 147; f) W. S. Ahn, D. H. Lee, T. J. Kim, J. H. Kim, G. Seo, R. Ryoo, *Appl. Catal. A* **1999**, *181*, 39 – 49; g) M. S. Morey, S. O'Brien, S. Schwarz, G. D. Stucky, *Chem. Mater.* **2000**, *12*, 898 – 911.

[5] a) A. Vinu, P. Srinivasu, M. Miyahara, K. Ariga, *J. Phys. Chem. B* **2006**, *110*, 801 – 806; b) B. François, K. Abdelkarim, T. J. Michael, K. Freddy, S. Kaliaguine, *Indust. Chem. Res.* **2010**, *49*, 6977 – 6985.

[6] a) P. Wu, M. Iwamoto, *J. Chem. Soc. Faraday Trans.* **1998**, *94*, 2871 – 2875; b) R. D. Oldroyd, J. M. Thomas, T. Maschmeyer, P. A. MacFaul, D. W. Snelgrove, K. U. Ingold, D. D. M. Wayner, *Angew. Chem.* **1996**, *108*, 2966 – 2969; *Angew. Chem. Int. Ed. Engl.* **1996**, *35*, 2787 – 2790; c) Z. Hua, W. Bu, Y. Lian, H. Chen, L. Li, L. Zhang, C. Li, J. J. Shi, *J. Mater. Chem.* **2005**, *15*, 661 – 665; d) F. Bérubé, B. Nohair, F. Kleitz, S. Kaliaguine, *Chem. Mater.* **2010**, *22*, 1988 – 2000; e) M. Reichinger, W. Schmidt, M. W. E. van den Berg, A. Aerts, J. A. Martens, C. E. A. Kirschhock, H. Gies, W. Grünert, *J. Catal.* **2010**, *269*, 367 – 375.

[7] X. Y. Yang, Y. Han, K. Lin, G. Tian, Y. F. Feng, X. J. Meng, Y. Di, Y. Du, Y. Zhang, F. S. Xiao, *Chem. Commun.* **2004**, 2612 – 2613.

[8] a) Y. Han, F. S. Xiao, S. Wu, Y. Y. Sun, X. J. Meng, D. S. Li, S. Lin, *J. Phys. Chem. B* **2001**, *105*, 7963 – 7966; b) S. Wu, Y. Han, Y. C. Zou, J. W. Song, L. Zhao, Y. Di, S. Z. Liu, F. S. Xiao, *Chem. Mater.* **2004**, *16*, 486 – 492; c) D. Serrano, R. Sanz, P. Pizarro, I. Moreno, *Chem. Commun.* **2009**, 1407 – 1409.

[9] a) W. Peng, J. F. Ruan, L. L. Wang, L. L. Wu, Y. Wang, Y. M. Liu, W. B. Fan, M. Y. He, O. Terasaki, T. Tatsumi, *J. Am. Chem. Soc.* **2008**, *130*, 8178 – 8187; b) L. L. Wang, Y. Wang, Y. M. Liu, H. H. Wu, X. H. Li, M. Y. He, P. Wu, *J. Mater. Chem.* **2009**, *19*, 8594 – 8602.

[10] a) Y. R. Wang, M. Lin, A. Tuel, *Microporous Mesoporous Mater.* **2007**, *102*, 80 – 85; b) N. J. Guan, Y. S. Han, *Chem. Lett.* **2000**, 1084 – 1085.

[11] a) J. L. Blin, A. Leonard, Z. Y. Yuan, L. Gigot, A. Vantomme, A. K. Cheetham, B. L. Su, *Angew. Chem.* **2003**, *115*, 2978 – 2981; *Angew. Chem. Int. Ed.* **2003**, *42*, 2872 – 2875; b) Z. Y. Yuan, T. Z. Ren, B. L. Su, *Adv. Mater.* **2003**, *15*, 1462 – 1465; c) Z. Y. Yuan, B. L. Su, *J. Mater. Chem.* **2006**, *16*, 663 – 677; d) B. L. Su, A. Vantomme, L. Suarhy, R. Pirard, J. P. Pirard, *Chem. Mater.* **2007**, *19*, 3325 – 3333; e) X. Y. Yang, Y. Li, G. Van Tendeloo, F. S. Xiao, B. L. Su, *Adv. Mater.* **2009**, *21*, 1368 – 1372; f) X. Y. Yang, A. Leonard, A. Lemaire, G. Tian, B. L. Su, *Chem. Commun.* **2011**, *47*, 2763 – 2786.

[12] a) B. Notati, *Catal. Today* **1993**, *18*, 163; b) K. T. Jung, Y. G. Shul, *Chem. Mater.* **1997**, *9*, 420 – 422; c) Y. Cheneviere, F. Chieux, V. Caps, A. Tuel, *J. Catal.* **2010**, *269*, 161 – 168.

[13] W. B. Fan, R. G. Duan, T. Yokoi, P. Wu, Y. Kunota, T. Tatsumi, *J. Am. Chem. Soc.* **2008**, *130*, 10150 – 10164.

[14] J. Zhou, Z. L. Hua, X. Z. Cui, Z. Q. Ye, F. M. Cui, J. L. Shi, *Chem. Commun.* **2010**, *46*, 4994 – 4996.

